Experiments in Fluids 25 (1998) 16–22 © Springer-Verlag 1998

Experiments on the lift of a spinning sphere in a range of intermediate Reynolds numbers

B. Oesterlé, T. Bui Dinh

Abstract The lift force experienced by a spinning sphere moving in a viscous fluid, with constant linear and angular velocities, is measured by means of a trajectographic technique. Measurements are performed in the range of dimensionless angular velocities $\gamma = a\omega/V$ lying between 1 and 6, and in the range of Reynolds numbers $Re = 2aV/\nu$ lying between 10 and 140 (a sphere radius, ω angular velocity, V relative velocity of the sphere centre, ν fluid kinematic viscosity). A notable departure from the theoretical relationship at low Reynolds number, $C_L = 2\gamma$, is obtained, the ratio C_L/γ being found to significantly decrease with increasing γ and increasing Re. The following correlation is finally proposed to estimate the lift coefficient in the range $10 < Re < 140$:

$$C_L \cong 0.45 + (2\gamma - 0.45)\exp(-0.075\gamma^{0.4}Re^{0.7})$$

1 Introduction

The prediction of the force exerted by a fluid on a suspended particle is of great interest for the study of suspension flows, which concerns many industrial fields, such as pneumatic transport, chemical engineering or environmental mechanics. In the case of solid particles conveyed in a confined fluid flow, significant spinning motion may be induced by particle–wall collisions or particle–particle collisions. It is therefore necessary to know the influence of the spinning motion on the force and on the torque undergone by a particle. In particular, the lift force arising from particle spin must generally be taken into account in order to perform trajectory calculations in Lagrangian modelling, or to express the fluid–particle interaction terms when using Eulerian formulations. In the present paper, we are interested in the lift force exerted on a spinning spherical particle in a finite range of moderate Reynolds numbers, which are frequently encountered in suspension flows.

Received: *20 May 1996*/*Accepted*: *9 November 1997*

B. Oesterlé, T. Bui Dinh[1]
Laboratoire Universitaire de Mécanique et d'Energétique de Nancy (LUMEN) ESSTIN, Université Henri Poincaré, Nancy 1, F-54500 Vandoeuvre-les-Nancy, France

Correspondence to: B. Oesterlé

[1]*Present address*: Institute of Mechanics, Hanoi, Vietnam

The hydrodynamical force on a moving body is usually resolved into the drag force F_D, in the direction of the relative motion, and the lift force F_L, which is orthogonal to the direction of the relative motion. These force components are characterized by the dimensionless coefficients C_D and C_L, defined by

$$C_D = \frac{F_D}{\frac{1}{2}\rho V^2 A} \tag{1}$$

$$C_L = \frac{F_L}{\frac{1}{2}\rho V^2 A} \tag{2}$$

where ρ is the fluid density, V is the magnitude of the relative velocity, and A is the frontal area of the body. In a similar manner, the dimensionless torque coefficient can be defined by

$$C_T = \frac{T}{\frac{1}{2}\rho V^2 A a} \tag{3}$$

where T is the torque and a denotes a reference length.

Under steady conditions, and in a fluid with constant density and constant kinematic viscosity ν, it can be shown by dimensional analysis that these coefficients depend on the Reynolds number $Re = 2aV/\nu$ and on the dimensionless rotational velocity $\gamma = a\omega/V$, where ω stands for the angular velocity, which is assumed to be normal to the relative translation velocity. Unfortunately, even in the case of the simpler shape, which is the spherical one, very few results are known, especially at intermediate Reynolds numbers. The range of very small Reynolds numbers was theoretically investigated by Rubinow and Keller (1961), by means of matched asymptotic expansions. In this case, C_D is independent of γ, whereas the lift and torque coefficients are found to be

$$C_L = 2\gamma(1 + O(Re)) \tag{4}$$

$$C_T = \frac{32\,\gamma}{Re}(1 + o(Re)) \tag{5}$$

where the symbol O means that the ratio $O(Re)/Re$ remains bounded as $Re \to 0$, and the symbol o means instead that the ratio $o(Re)/Re$ tends to zero as $Re \to 0$. In Eqs. (4) and (5), the reference length a is the sphere radius, and the reference area A is πa^2. Note that Eq. (5) means that the torque does not depend on the linear velocity V when $Re \to 0$. Dennis et al. (1980) calculated the torque on a rotating sphere in a fluid

at rest. Since C_T cannot be defined as above when $V=0$, a modified dimensionless torque coefficient was computed in terms of the rotation Reynolds number (or Taylor number) $Re_\omega = \frac{1}{2}\gamma Re$. The corresponding prediction agrees very well with the measurements of Sawatzki (1970). Appreciable deviation from Eq. (5) can be observed when $Re_\omega > 10$.

On the other hand, a number of experimental results concerning the lift force on a spinning sphere were obtained at high Reynolds numbers ($Re > 10^4$), especially by Maccoll (1928), Davies (1949) and Tani (1950): in that range, the lift coefficient is almost independent of the Reynolds number, and much lower than predicted by Eq. (4). At low spinning rate, a negative lift may occur, as first pointed out by Maccoll (1928). Such an effect was confirmed by Tanaka et al. (1990) in the Reynolds number range from 6×10^4 to 1.5×10^5. However, such large Reynolds numbers do not belong to the range we are dealing with in the present paper.

In the range of moderate Reynolds numbers, lying between 1 and 10^4, much less information is available. The only known works concerning the lift on a spinning sphere at such Reynolds numbers are the experimental studies of Barkla and Auchterlonie (1971) and Tsuji et al. (1985), and the numerical investigation by Chegroun and Oesterlé (1993). Using a conical pendulum technique, Barkla and Auchterlonie (1971) estimated the lift and drag coefficient of a rotating sphere in the range $1500 < Re < 3000$. The lift coefficient was found to be roughly proportional to γ for $\gamma > 5$, the coefficient of proportionality being 0.09 ± 0.02. At lower values of γ, the ratio C_L/γ was increasing with decreasing γ ($C_L/\gamma \approx 0.16 \pm 0.04$ in the range $2 < \gamma < 4$). Another technique has been used by Tsuji et al. (1985), who studied the trajectories of spheres bouncing on an inclined plate. The relation between lift and spin was determined by measuring the angular velocity from stroboscopic photographs, and comparing the recorded trajectories with calculated trajectories which were computed assuming proportionality between C_L and γ. For Reynolds numbers between 550 and 1600, and dimensionless angular velocities less than 0.7, they proposed the following relationship

$$C_L = (0.40 \pm 0.10)\gamma \tag{6}$$

A numerical investigation in the range $0 < Re \leqslant 40$, performed by Chegroun and Oesterlé (1993), showed that the lift coefficient decreases with increasing Re at fixed γ. At low Reynolds numbers ($Re \leqslant 5$), the predicted values of C_L were approximately proportional to γ, however the ratio C_L/γ was found to significantly decrease with increasing Re for $Re > 5$. Nevertheless, such results need still to be confirmed and to be extended at higher Reynolds numbers.

This brief review shows that there is still a lack of information in the range $1 < Re < 500$, which corresponds, for instance, to the frequently encountered case of particles having a diameter between 0.1 and 1 mm, suspended in a gas or a liquid flow. That is the reason why we aimed at performing lift measurements at Reynolds numbers belonging to this intermediate range.

In this paper, we will first describe the original experimental technique we developed for such measurements. Complete results concerning the lift coefficient will then be given and discussed. The present results are compared with the above-mentioned previous works, and an empirical correlation for predicting the lift coefficient is finally proposed.

2
Experimental arrangement and method

As pointed out by Tsuji et al. (1985), direct measurement of the force acting on a spinning sphere is very difficult in the range of Reynolds numbers lower than 10^3, since it would need the use of a very small sphere, placed in a uniform liquid flow, and the transverse force would be too small to be measured. Moreover, such a direct method would involve a supporting device, including for instance an electric motor, which might lead to significant flow disturbance. The present experimental technique lies therefore on an indirect method, which consists in examining the trajectory of a sphere moving upwards in a liquid at rest. As can be seen in Fig. 1, the sphere is equipped with two very thin cylindrical axles, which are symmetrically fixed along a diametrical direction. A sketch of the experimental apparatus is given by Fig. 2. The motion is induced by means of a counterweight (M) and two suspension threads, which are coiled on the axles, yielding a rotational velocity which can be deduced from the measurements of the velocities of the sphere and of the counterweight (the latter being measured by means of the laser device shown on Fig. 2). Note that the lateral deviation of the sphere is exaggerated for the sake of clearness of the figure.

In order to allow the angular velocity of the sphere to be controlled and measured, sphere diameters of at least 1 cm were chosen. Moreover, the relative velocity of the sphere

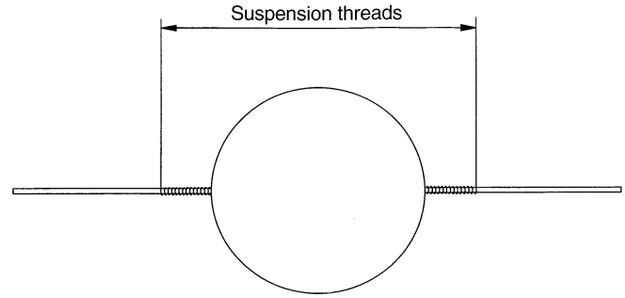

Fig. 1. Illustration of the sphere arrangement

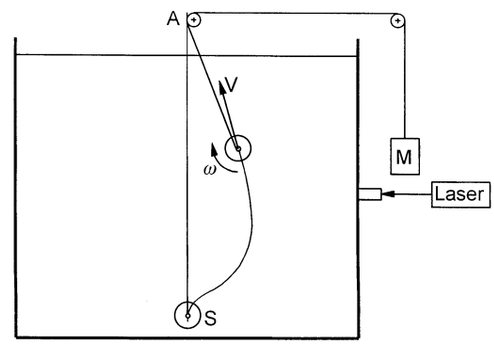

Fig. 2. Sketch of the experimental apparatus

centre with respect to the fluid should be high enough so that any possible free convection motion may be neglected. Under such conditions, Reynolds numbers ranging between 10 and 140 could be obtained by using a sufficiently viscous liquid, and the transverse force acting on the sphere could be detected and measured by analysing its trajectory, as will be shown hereafter.

2.1 Description of the motion of the sphere

The momentum conservation of the sphere yields the following general equation of motion, written under vectorial form:

$$(m+m_a)\frac{\mathrm{d}\mathbf{V}}{\mathrm{d}t}=m'\mathbf{g}+\mathbf{F}_L+\mathbf{F}_D+\mathbf{F}_T \tag{7}$$

where m and m_a are the mass and the added mass, respectively, of the sphere and the axles, and m' is the apparent mass of the sphere (including the axles), obtained by subtracting the mass of the liquid displaced from the total mass m, in order to account for the buoyancy force. $\mathbf{V}$ is the sphere velocity, $\mathbf{g}$ is the gravity acceleration, $\mathbf{F}_L$ and $\mathbf{F}_D$ are the lift and drag force vectors, and $\mathbf{F}_T$ denotes the tension of the suspension threads. Note that the lift and drag forces in Eq. (7) include the contribution of the cylindrical axles.

The conservation of angular momentum leads to

$$J\frac{\mathrm{d}\omega}{\mathrm{d}t}=-T+a_1F_T \tag{8}$$

where J is the moment of inertia of the moving body (sphere and axles), ω its angular velocity, F_T the magnitude of the tension of the threads, and a_1 denotes the coiling radius, which is the sum of the radii of the axle and of the thread.

Due to the presence of the fixed pulley A, the sphere reaches, after an acceleration phase giving rise to a lateral deviation, a steady rectilinear motion with constant linear and angular velocities, as illustrated in Fig. 3. During this steady-state phase, the equations of motion lead to the following simplified expressions of the lift, drag and torque, where φ denotes the angle between the straight trajectory and the vertical direction:

$$F_L=m'g\sin\varphi \tag{9}$$

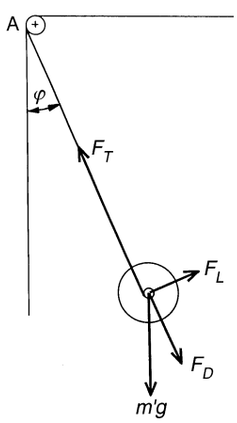

Fig. 3. Upward motion of the sphere in the straight part of the trajectory

$$F_D=F_T-m'g\cos\varphi \tag{10}$$

$$T=a_1F_T \tag{11}$$

Because of the friction at the pulleys, the force F_T is not accurately known, so that the drag force and the torque unfortunately cannot be measured by the present technique. On the contrary. Eq. (9) shows that the lift force can be directly derived from the measurement of the angle φ, keeping in mind that the result must be corrected to take into account the lift due to the axles (as described farther).

The main advantage of this experimental procedure lies in the fact that the linear and angular velocities of the sphere can be controlled by the choice of sphere diameter and density, axle diameter and counterweight mass. Furthermore, the behaviour of the sphere during the steady rectilinear phase of the trajectory does not depend on the initial conditions. This technique makes it possible to provide new results under steady-state conditions, unlike the previous experiments performed at $Re<10^4$, referred to in the Introduction to this paper. It must be pointed out, however, that the proposed method is restricted to the range of moderate Reynolds numbers investigated herein. Experiments at higher Reynolds numbers (10^3–10^4) were unfortunately not possible, since such measurements would require a very large tank in order that the steady rectilinear motion could be reached, due to the sphere inertia increase involved by larger diameter or higher velocity.

2.2 Experimental data and procedure

Results presented hereafter were obtained in a tank of 1×1 m side and 1.2 m depth, filled with a vegetable oil of density 901 kg/m^3, and whose viscosity, lying between 0.07 and 0.09 Pa s, was carefully measured in terms of temperature. The motion of the sphere could be observed through a plexiglass window which is the front wall of the tank. The sphere trajectories were photographically recorded under stroboscopic illumination, supplied by a Xenon flash tube (flash duration about 80 μs). The frequency of the strobe light was set at 10 flashes/s.

Five lathe-turned, polished spheres were used, the characteristics of which are shown in Table 1. Cylindrical steel axles have

Table 1. Summary of test conditions and run references

Sphere material	Sphere diameter [mm]	Axle diameter [mm]	Mass [g]	Thread diameter [mm]	Run reference
Brass	17.0	1.00	24.150	0.08	Ba
				0.12	Bb
		1.00	24.302	0.12	Bc
		1.50	27.020	0.12	Bd
Duralumin	30.2	1.50	42.192	0.08	Da
				0.12	Db
		2.00	49.374	0.12	Dc
	55.1	1.50	251.26	0.12	Dd
		2.00	252.10	0.12	De
Titanium	25.0	1.50	39.170	0.12	Ta
				0.18	Tb
	38.8	1.50	138.544	0.18	Tc

been symmetrically fixed on each side of the sphere, the length of each part lying between 72 and 92 mm. The ratio of the axle diameter to the sphere diameter ranged from 0.038 to 0.088. The diameters of the suspension filaments (nylon threads) were 0.08, 0.12 or 0.18 mm, depending on the mass of the sphere.

Before each experiment, the sphere is placed on the bottom of the tank (starting point S) by means of a moving supporting device (electric motor and endless screw), and the position of the pulley is adjusted in such a manner that the line AS is perfectly vertical (A being the point of contact between the thread and the pulley). After waiting for the liquid to be perfectly still, the sphere is released with zero initial linear and angular velocity, and its trajectory is recorded. The counterweight velocity V_c is simultaneously measured by a laser device, which may be vertically displaced in order to insure that the measurement is performed during the straight part of the sphere trajectory. The sphere velocity V, as well as the angle φ between the rectilinear trajectory and the vertical direction, are obtained directly from the trajectory analysis using a digitizing table. For the sake of preciseness in photograph readings, each trajectory is first recorded without spinning of the sphere, so that any uncertainty due to the scale of the picture and to the stroboscope frequency can be eliminated using the known data concerning the drag coefficient of a non-spinning sphere (as given by the expression proposed by Morsi and Alexander, 1972). The angular velocity of the sphere is then calculated by

$$\omega = \frac{V_c - V}{a_1} \tag{12}$$

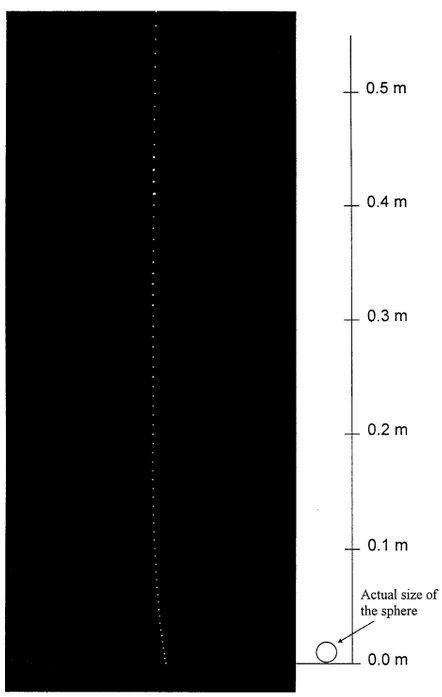

Fig. 4. Example of trajectory photograph ($Re = 22.42$, run reference Ba6, see Table 1)

A typical example of trajectory photograph, showing the lateral deviation due to the sphere rotation, is given in Fig. 4. It must be emphasized that the light-spots on the photograph represent only a small part of the sphere, since they are due to the reflection of the flashes by the polished spherical surface. As can be seen on the reference scale on the right of the figure, which gives also the actual size of the sphere, the field of view of the photograph covers about the half of the depth of the tank. Measurements of V and φ, which were generally performed between $\frac{1}{3}$ and $\frac{1}{2}$ of the full height of the tank, are deduced from coordinate readings of two points $\mathbf{P}_1$, $\mathbf{P}_2$, belonging to the rectilinear part of the trajectory. The assumption of steady rectilinear motion of the sphere is checked by comparing the distances between two successive spots in the lower and higher part of the path $\mathbf{P}_1\mathbf{P}_2$: if the discrepancy exceeds 5%, the measurement is rejected. The accuracy of the measurements will be discussed below.

2.3 Lift correction and uncertainty assessment

In order to account for the presence of the axles, the measured lift force F_{Lm} is corrected by subtracting the lift force due to the axles, that is:

$$F_L = F_{Lm} - F_{La} \tag{13}$$

where F_L is the lift of the sphere and F_{La} is the lift of the cylindrical axles. The corresponding correction for the lift coefficient is written:

$$C_L = C_{Lm} - C_{L,\,\mathrm{cyl}} \frac{2a_{\mathrm{cyl}}l}{\pi a^2} \tag{14}$$

where a_{cyl} and l are the radius and the total length of the axles, respectively. $C_{L,\,\mathrm{cyl}}$ is the lift coefficient of the axles, which can be estimated from the work of Ingham and Tang (1990), who numerically calculated the lift of a rotating circular cylinder at Reynolds numbers $Re_{\mathrm{cyl}} = 5$ and $Re_{\mathrm{cyl}} = 20$ (based on cylinder diameter). The predicted lift coefficients were $C_{L,\,\mathrm{cyl}} = 2.77\gamma_{\mathrm{cyl}}$ at $Re_{\mathrm{cyl}} = 5$, and $C_{L,\,\mathrm{cyl}} = 2.54\gamma_{\mathrm{cyl}}$ at $Re_{\mathrm{cyl}} = 20$, where $\gamma_{\mathrm{cyl}} = a_{\mathrm{cyl}}\omega/V$ is the dimensionless angular velocity of the cylinder, in the range of $0 \leqslant \gamma_{\mathrm{cyl}} \leqslant 3$.

In our experiments, γ_{cyl} lies between 0 and 0.5, and the cylinder Reynolds number is in the range $0.5 \leqslant Re_{\mathrm{cyl}} \leqslant 5$. Therefore, we decided to adopt the result obtained by Ingham and Tang (1990) at $Re_{\mathrm{cyl}} = 5$, namely $C_{L,\,\mathrm{cyl}} = 2.77\gamma_{\mathrm{cyl}}$. Numerical calculations of the lift correction using such an estimate show that the lift due to the axles is 6–14% of the total measured lift, so that a 10% error in the cylinder lift leads to an uncertainty of about 1% in the sphere lift estimate.

Our uncertainties that must be taken into account are mainly due to the inaccuracies in the measurements of the angle φ and of the sphere velocity V. Considering that the lift coefficient is inversely proportional to V^2, and proportional to $\sin\varphi$ (with $\varphi \ll 1$), the relative error in C_{Lm} is given as follows:

$$\frac{\Delta C_{Lm}}{C_{Lm}} \cong \frac{\Delta\varphi}{\varphi} + 2\frac{\Delta V}{V} \tag{15}$$

where $\Delta\varphi/\varphi$ and $\Delta V/V$ are about 10% and 5%, respectively, according to repeated digitizing tests intended to assess the preciseness of coordinate readings. As a consequence, it can be

considered that the measured values for the lift coefficient are accurate to about 20%.

According to Eq. (12), the angular velocity uncertainty can be expressed as

$$\frac{\Delta\omega}{\omega}=\frac{\Delta V_c+\Delta V}{|V_c-V|}+\frac{\Delta a_1}{a_1} \tag{16}$$

where $\Delta V_c/V_c$ and $\Delta a_1/a_1$ are approximately 2%. Due to the denominator $|V_c-V|$, the first term of the r.h.s. in Eq. (16), which may reach about 15%, is a major source of error. Therefore, taking into account $\Delta\gamma/\gamma=\Delta\omega/\omega+\Delta V/V$, the uncertainty in determining the dimensionless angular velocity γ can be roughly estimated to 20%.

Such a large uncertainty could conceivably have been avoided in using some device allowing the angular velocity to be directly obtained from the photographs, like segments marked on the sphere surface, as was used by Tsuji et al. (1985). So far, such a method was not possible in the present experiments, due to lighting problems which could not be suppressed completely: in particular, as shown by Fig. 4, the stroboscopic illumination produces only a small light-spot on the spherical surface, which is not broad enough to detect any rotational motion of the sphere.

3 Results and discussion

All test conditions are summarized in Table 1, and detailed experimental results, which cover the ranges $10<Re<140$ and $1<\gamma<6$, are listed in the Appendix. In order to compare the dependence of the lift coefficient upon the dimensionless angular velocity with the theoretical result of Rubinow and Keller (1961), and to study the influence of the Reynolds number, it was decided to split the range $10<Re<140$ into six subranges, and to plot C_L as a function of γ in each Reynolds number subrange.

Corresponding results are displayed in Fig. 5a–c, where the solid lines illustrate the Rubinow and Keller's relationship, $C_L=2\gamma$, valid at small Reynolds numbers. In spite of some scatter in the experimental results, the present measurements reveal the tendency to obtain lower lift coefficients at higher values of the Reynolds number. At the lower Reynolds numbers investigated here (Fig. 5a), the lift coefficient can be seen to be approximately proportional to the dimensionless angular velocity. However, such a linear variation of C_L with γ does not exist at higher Reynolds numbers, as shown by Fig. 5c. The dispersion of the results, which is particularly high in the range $40<Re<80$, may exceed the estimated uncertainty since it is not only due to the above-quantified inaccuracy on measured lift coefficients and angular velocities (which are illustrated by error bars for the outermost points), but also to some inescapable irregularities in the sphere trajectories, or to possible influence of the suspension threads. Unfortunately, no attempt could be made to evaluate such effects.

As can be seen in Fig. 6, which is a plot of the lift coefficient as a function of the Reynolds number, the present data compare favourably with the numerical predictions by Chegroun and Oesterlé (1993), which are restricted to $Re\leqslant 40$. In particular, the numerically predicted influence of the spinning rate, as well as the effect of the Reynolds number, are

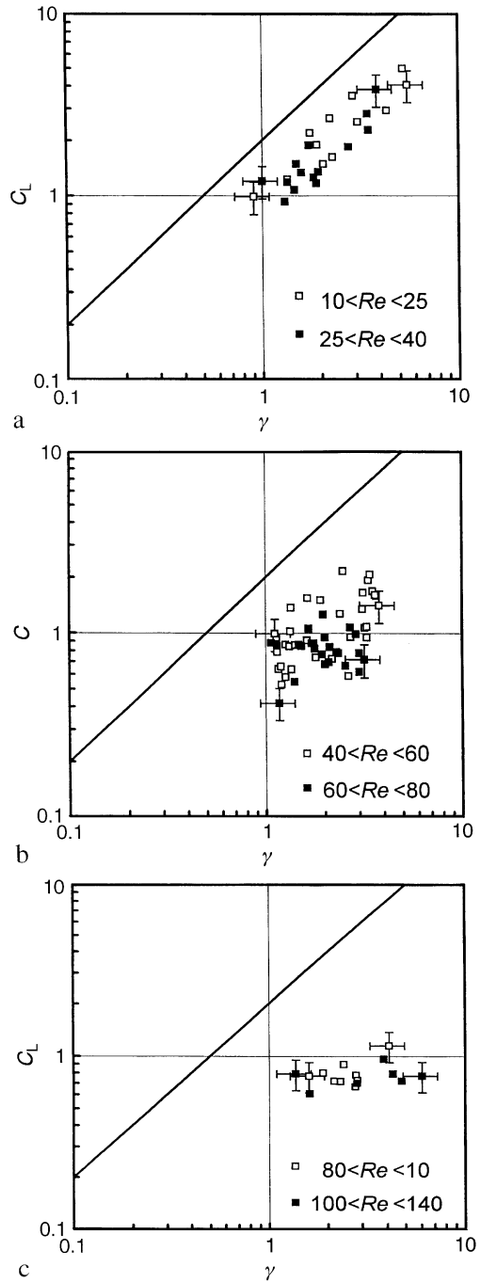

Fig. 5a–c. Measured lift coefficient as a function of the dimensionless angular velocity γ (solid lines refer to Rubinow and Keller's theoretical result). **a** $10<Re<40$; **b** $40<Re<80$; **c** $80<Re<140$

qualitatively confirmed by the present experiments: C_L can be seen to decrease with decreasing γ or increasing Re. Moreover, the experimental results seem to indicate that the influence of γ vanishes for Reynolds numbers exceeding about 100. At such values of Re, the lift coefficient is very slightly decreasing with increasing Re. Regarding the flow structure, the numerical predictions show that the recirculation region, due to the separation which is known to take place for $Re>20$ for the non rotating sphere (Taneda 1956; Dennis and Walker 1971),

disappears as soon as the sphere is rotating, owing to the no-slip condition at the sphere surface. For the same reason, the location of the stagnation point is displaced at a distance from the sphere, and a rotating layer exists close to the boundary. Although no information about the flow structure can be provided by the present experiments, this phenomenon may explain the significant dependency of the lift upon *Re* in the range investigated here, due to the crucial changes in the pressure field and shear stress distribution at the rear side of the sphere which occur at such intermediate Reynolds numbers. Further numerical calculations are needed in order to clarify this point.

In spite of the noisy character of the experimental data, it is possible to propose an approximate relationship expressing the lift coefficient in terms of γ and *Re*, provided that the suggested correlation matches the theoretical expression given by Eq. (4) at low Reynolds numbers, as well as the experimental results obtained by Barkla and Auchterlonie (1971) and by Tsuji et al. (1985) at higher Reynolds numbers. The best fit is given by the following correlation:

$$C_L \cong 0.45 + (2\gamma - 0.45)\exp(-0.075\gamma^{0.4}Re^{0.7}) \qquad (17)$$

In Fig. 7, Eq. (17) is plotted for $\gamma = 1$; 2; 3 and 4, together with the experimental values of the ratio C_L/γ. The figure shows that the complete range of Reynolds numbers up to about 2000 can be described using the suggested correlation, which has the proper limiting behaviour for both small and high Reynolds numbers. Notwithstanding the scatter in the data, the unambiguous decrease of the ratio C_L/γ with increasing γ and increasing *Re* is satisfactorily described by Eq. (17), which may therefore be expected to provide some improvements in the prediction of the lift of spinning particles in suspension flows. However, considering the lack of data for $Re > 140$, it is suggested to restrict the use of Eq. (17) in the range $10 < Re < 140$.

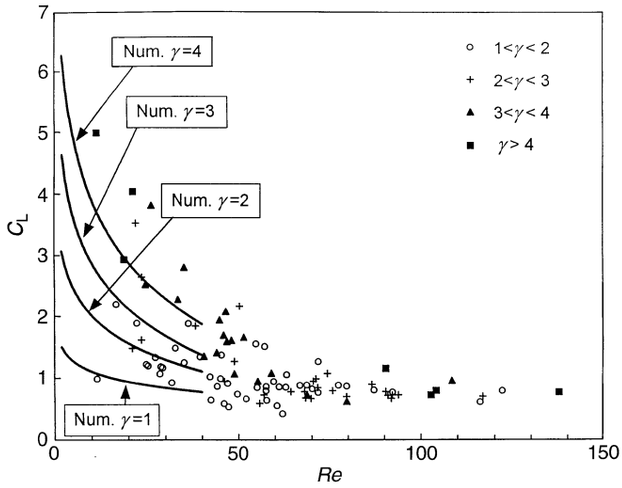

Fig. 6. A plot of the lift coefficient as a function of the Reynolds number. Symbols refer to the present experiments, and solid lines refer to the numerical results of Chegroun and Oesterlé (1993)

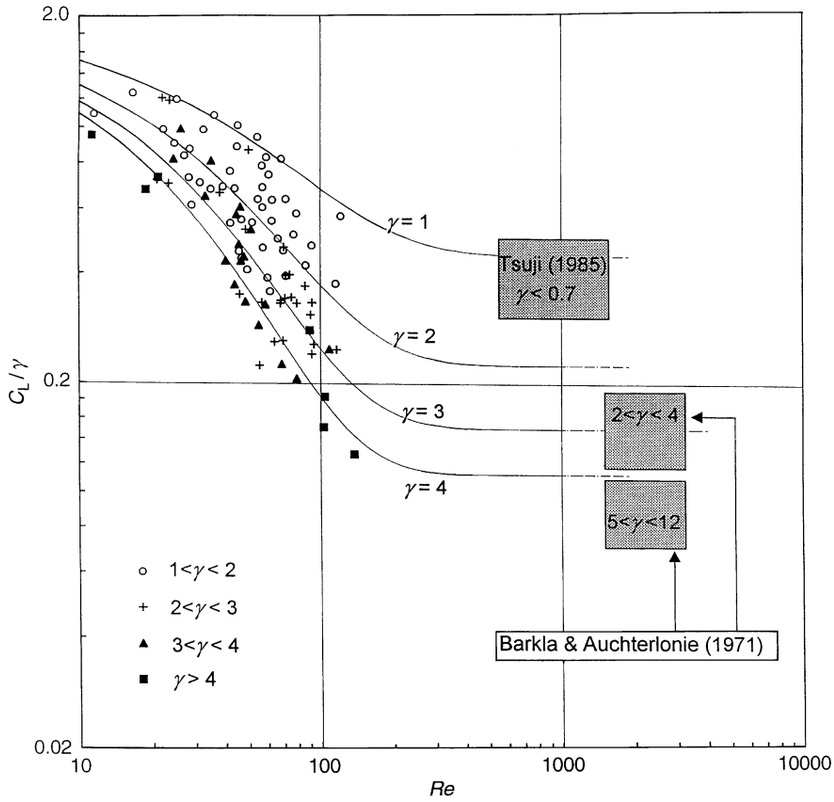

Fig. 7. A plot of the ratio C_L/γ as a function of the sphere Reynolds number *Re*. Present results (symbols) are compared to the experimental results by Tsuji et al. (1985) and Barkla and Auchterlonie (1971), depicted by shaded areas, and to the proposed correlation, given by Eq. (17), for $\gamma = 1$; 2; 3 and 4 (lines)

4 Conclusion

Results concerning the lift experienced by a spinning sphere moving in a viscous fluid have been obtained by means of a trajectographic technique, which was shown to be able to provide new interesting information which is necessary, for instance, for the computation of particle trajectories in suspension flows. The lift coefficient has been measured under steady-state conditions, in the range of sphere Reynolds numbers $10 < Re < 140$ and for dimensionless angular velocities γ ranging from 1 to 6.

Despite of the difficulty to get very accurate measurements, the influence of the Reynolds number and of the dimensionless angular velocity has been pointed out, and a new empirical correlation has been proposed for the lift coefficient in the range $10 < Re < 140$. It is suggested that this original correlation should be used in order to supplement the previously existing results of Rubinow and Keller (1961), Tsuji et al. (1985) or Barkla and Auchterlonie (1971).

Any explanation of the behaviour of the lift coefficient in terms of both γ and Re would require further information concerning the flow structure around the sphere. That is the reason why additional investigation is currently being carried out by means of numerical calculations, in order to discuss the observed results with relevance to the changes which take place in the velocity and pressure fields.

Appendix

Run n°[1]	Re	γ	C_L	Run n°	Re	γ	C_L
Ba1	11.36	5.250	4.986	Bc13	55.28	1.325	0.847
Ba2	11.55	0.905	0.985	Ta2	55.40	3.285	0.949
Ba3	16.73	1.765	2.197	Dd5	55.89	2.635	0.590
Ba4	19.01	4.335	2.930	Tb9	57.08	2.180	0.726
Ba5	21.12	2.055	1.480	Bc14	57.34	1.910	1.506
Ba6	21.40	5.530	4.040	Bc15	57.69	1.145	0.790
Ba7	22.12	2.925	3.530	Dc6	57.71	1.415	0.860
Ba8	22.42	1.910	1.886	Tb10	57.84	1.355	0.638
Ba9	23.60	2.295	1.615	Ta3	59.12	3.285	1.080
Ba10	23.69	2.230	2.650	Tb11	59.81	1.135	0.945
Db1	24.69	3.080	2.529	Tb12	60.58	1.405	0.548
Ba11	24.94	1.350	1.220	Tb13	61.24	1.145	0.855
Ba12	25.45	1.000	1.196	Tb14	62.05	1.175	0.420
Bd1	26.36	3.850	3.819	Tb15	63.03	1.525	0.852
Ba13	27.41	1.590	1.330	Bc16	63.35	1.660	1.057
Ba14	28.65	1.465	1.070	Tb16	64.41	2.995	0.780
Ba15	28.84	1.350	1.179	Tb17	66.92	1.760	0.878
Bc1	29.40	1.895	1.166	Tb18	68.17	2.350	0.780
Bc2	31.82	1.305	0.925	Tb19	68.38	2.010	0.678
Bc3	32.78	1.500	1.483	Tb20	68.81	1.070	0.883
Tb1	33.43	3.495	2.278	Dc7	68.83	3.185	0.720
Bd2	35.27	3.460	2.808	Tb21	69.85	2.545	0.667
Da1	35.30	1.838	1.250	Tb22	70.28	1.780	0.823
Tb2	36.38	1.735	1.881	Tb23	70.58	2.005	0.948
Bd3	38.34	2.765	1.840	Dc8	71.33	2.890	0.988
Bc4	39.62	1.940	1.341	Tb24	71.86	2.125	0.841
Bc5	40.58	3.115	1.350	Tb25	71.94	1.940	0.765
Tb3	42.31	1.340	1.020	Dc9	72.00	1.970	1.262
Bc6	42.47	1.165	0.640	Tb26	74.45	2.700	1.072
Bc7	44.14	3.785	1.410	Tb27	75.83	2.295	0.790
Tb4	44.29	1.265	0.865	Dc10	77.53	1.720	0.880
Dc1	44.84	3.340	1.940	Tc1	79.64	3.005	0.619
Bc8	45.17	1.115	0.990	Ta4	79.67	2.100	0.697
Tb5	45.46	1.350	1.372	Tb28	79.73	1.475	0.865
Dc2	46.01	3.520	1.690	Tb29	86.63	2.415	0.895
Tb6	46.08	1.265	0.581	Dc11	87.15	1.895	0.800
Bc9	46.25	2.710	0.950	Tc2	90.45	2.795	0.777
Bb1	46.56	3.410	2.080	De1	90.57	4.110	1.150
Bb2	46.95	3.670	1.590	Tc3	91.04	2.320	0.716
Tb7	47.18	1.625	0.912	Tc4	91.94	2.770	0.667
Bc10	47.30	1.205	0.530	Tc5	92.28	2.155	0.718
Bb3	48.16	3.620	1.610	Tb30	92.33	1.605	0.767
Dc3	48.94	3.200	1.070	Tc6	93.88	2.835	0.726
Tb8	48.99	2.405	1.270	Dd1	102.83	4.765	0.720
Dc4	49.81	1.800	0.737	Dd2	104.21	4.305	0.790
Bb4	50.39	2.490	2.170	De2	108.60	3.860	0.960
Ta1	51.61	3.145	1.660	Tc7	116.15	1.615	0.607
Bc11	52.25	1.195	0.660	Dd3	116.86	2.825	0.700
Bc12	54.93	1.640	1.550	Tc8	122.18	1.370	0.791
				Dd4	137.82	6.050	0.770

[1]See Table 1 for run references

References

Barkla HM; Auchterlonie LJ (1971) The Magnus or Robins effect on rotating spheres. J Fluid Mech 47: 437–447

Chegroun N; Oesterlé B (1993) Etude numérique de la traînée, de la portance et du couple sur une sphère en translation et en rotation. Actes 11ème Congrès Français de Mécanique, Lille-Villeneuve d'Ascq, France, 3: 81–84

Davies JM (1949) The aerodynamics of golf balls. J Appl Phys 20: 821–828

Dennis SCR; Singh SN; Ingham DB (1980) The steady flow due to a rotating sphere at low and moderate Reynolds numbers. J Fluid Mech 101: 257–279

Dennis SCR; Walker JDA (1971) Calculation of the steady flow past a sphere at low and moderate Reynolds numbers. J Fluid Mech 48: 771–789

Ingham DB; Tang T (1990) A numerical investigation into the steady flow past a rotating cylinder at low and intermediate Reynolds numbers. J Comput Phys 87: 91–107

Maccoll JH (1928) Aerodynamics of a spinning sphere. J Roy Aero Soc 32: 777–798

Morsi SA; Alexander AJ (1972) An investigation of particle trajectories in two-phase flow systems. J Fluid Mech 55: 193–208

Rubinow SI; Keller JB (1961) The transverse force on a spinning sphere moving in a viscous fluid. J Fluid Mech 11: 447–459

Sawatzki O (1970) Das Strömungsfeld um eine rotierende Kugel. Acta Mechanica 9: 159–214

Tanaka T; Yamagata K; Tsuji Y (1990) Experiment of fluid forces on a rotating sphere and spheroid. Proc. of the 2nd KSME-JSME Fluids Engineering Conference, Seoul, Korea, October 10–13

Taneda S (1956) Studies on wake vortices (III). Experimental investigation of the wake behind a sphere at low Reynolds numbers. Reports of Research Institute for Applied Mechanics, Kyushu University, IV, 99–105

Tani I (1950) Baseball's curved balls. Kagaku (Science, in Japanese) 20: 405–409

Tsuji Y; Morikawa Y; Mizuno O (1985) Experimental measurement of the Magnus force on a rotating sphere at low Reynolds numbers. Trans A.S.M.E. J Fluids Engng 107: 484–488